

Variations in major aerosol components from long-term measurement of columnar aerosol optical properties at a SKYNET site downwind of Seoul, Korea

Yongjoo Choi, Young Sung Ghim*

Department of Environmental Science, Hankuk University of Foreign Studies, Yongin, 17035, Republic of Korea

HIGHLIGHTS

- Interpretation of variations in optical properties in terms of those in aerosol components.
- Comparing the results with those based on *in-situ* measurement data.
- Long-term trends during the past decade in which numerous measures were implemented.
- Potential source regions for both high and low values of optical properties.

ARTICLE INFO

Keywords:

Monthly variations
Long-term trends
Potential source regions
Long-range transport
Secondary formation

ABSTRACT

We investigated the variations in major aerosol components using optical properties from a SKYNET site downwind of metropolitan Seoul under prevailing westerlies. The study period was March 2007 through February 2017 during which numerous measures to reduce air pollutants were implemented in both Korea and China. Major aerosol components, including mineral dust (MD), secondary inorganic ions (SII), and carbonaceous materials were estimated from optical properties, such as fine mode volume fraction (FMVF), single scattering albedo (SSA), and the difference of absorption aerosol optical depth (dAAOD) between 400 and 870 nm. Monthly variations in aerosol characteristics estimated from the optical properties were mostly consistent with the previous studies based on *in-situ* measurement data. As many studies reported the reduction of particulate matter (PM) in Northeast Asia, AOD also decreased along with the reductions of MD and SII. Secondary formation during the long-range transport played an important role in elevating AOD. However, for the specific case of high FMVF, high SSA, or low dAAOD, potential source regions of aerosols tended to be distributed in the eastern Korean Peninsula and over the East Sea, as the effects of local emissions became larger than those of long-range transport. Although AOD variations successfully revealed the overall characteristics of PM on the whole, in some cases, the variations of optical properties were not clearly related to those of aerosol components.

1. Introduction

Over the past few years, particulate matter (PM) has become a major societal issue in Korea. The public's concern about PM_{2.5} was triggered by the nationwide high concentrations in early 2013 (Kim et al., 2016; Koo et al., 2018; Ghim et al., 2019) following unprecedented high concentrations in Beijing, China (Cheng et al., 2016; Fu and Chen, 2017; Huang et al., 2014; Ji et al., 2014; Tian et al., 2014; Wang et al., 2014a, 2014b). In the meantime, PM₁₀ and PM_{2.5} forecasts began (https://www.airkorea.or.kr/web/dustForecast?pMENU_NO=113, accessed

November 2019); countermeasures that had been taken against particulate matter were reorganized (<http://www.korea.kr/special/policyCurationView.do?newsId=148864591>, accessed November 2019); and a special act for particulate matter was legislated (<http://www.me.go.kr/home/web/board/read.do?menuId=286&boardMasterId=1&boardCategoryId=39&boardId=939205>, accessed November 2019). National air pollution monitoring networks are also being strengthened, a representative example being the expansion of the intensive monitoring network (KME, 2019). The intensive monitoring network is useful for investigating atmospheric processes involved in secondary productions

* Corresponding author.

E-mail address: ysghim@hufs.ac.kr (Y.S. Ghim).

<https://doi.org/10.1016/j.atmosenv.2020.117991>

Received 18 May 2020; Received in revised form 8 October 2020; Accepted 9 October 2020

Available online 13 October 2020

1352-2310/© 2020 Elsevier Ltd. All rights reserved.

as well as primary emissions, using online measurements of PM_{2.5} components and particle size distribution (NIER, 2009). However, the burden is that both the installation and operation of the equipment requires a considerable amount of expenses and skilled personnel.

During the past two decades ground-based remote sensing networks, such as Aerosol Robotic Network (AERONET) and Skyradiometer Network (SKYNET), have been rapidly expanded throughout the world (Holben et al., 1998, 2001; Nakajima et al., 2003, 2007; Campanelli et al., 2012; Zhang et al., 2012; Li et al., 2014; Hamill et al., 2016; Yoon et al., 2016; Arola et al., 2017). The strength of these networks is the ease of acquiring information from the ground through the standardization of measurements and data processing, which allows multi-year studies. This advantage is particularly important in East Asia, because most countries, including Korea, have only started monitoring PM_{2.5} in recent years, whereas the trend analysis using aerosol optical properties from remote sensing networks could use much longer data (de Meij et al., 2012; Collaud Coen et al., 2013; Li et al., 2014; Yoon et al., 2016). Furthermore, several research teams have attempted to identify chemical properties as well as physical properties, such as major aerosol types and chemical composition, from optical properties (Russell et al., 2010; Giles et al., 2012; Li et al., 2013, 2019; Choi et al., 2016; Choi and Ghim, 2016; Schuster et al., 2016; Xie et al., 2017; Zhang et al., 2018). Although the results from these studies are rough compared to those from *in-situ* measurements, they are useful enough in that they can provide information on chemical and physical properties of aerosols without much cost and efforts.

In this study, we analyze the variations in aerosol optical properties from the Yongin SKYNET site (YGN; 127.27° E, 37.34° N, 167 m asl) located at the Global Campus of Hankuk University of Foreign Studies for 10 years from March 2007 to February 2017. First, we investigate monthly variations in major aerosol components from those in optical properties based on the known relationships between them. Next, we explore the trends in optical properties and major aerosol components during the past decade when aerosol characteristics were revealed to have changed considerably due to environmental policies targeting particulate matter. Finally, we locate the potential source regions for high and low values of optical properties using the potential source contribution function (PSCF), which has been widely used for air quality study in East Asia (Guo et al., 2015; Kim et al., 2016; Jeong et al., 2017; Choi et al., 2020b). The last subject was assessed, considering that optical properties of columnar aerosols are more relevant to regional-scale variations and more suitable for PSCF analyses than *in-situ* measured properties of surface aerosols.

2. Methods

2.1. Skyradiometer and data processing

The skyradiometer, POM-02 (Prede Co. Ltd.) is an automatic sun-sky radiometer enabling the measurement of direct and diffuse solar radiation at 11 wavelengths (315, 340, 380, 400, 500, 675, 870, 940, 1020, 1600 and 2200 nm). Diffuse radiation was measured on the almucantar plane at 24 scattering angles, which was preprogrammed from 3° to 180° every 6 or 10 min. Direct radiation was measured at 1 min intervals when diffuse radiation was not measured. Among 11 wavelengths, radiation at five wavelengths of 400, 500, 675, 870 and 1020 nm was used in this study, because radiation at certain wavelengths is absorbed by ozone (315 nm), water vapor (940 nm), and cloud (1600 and 2200 nm), and because we need to obtain aerosol optical properties in a range similar to AERONET (440–1020 nm). Diffuse aerosol optical depths (AODs) were retrieved from almucantar measurements using skyrad. pack version 5 (Hashimoto et al., 2012). Direct AODs were obtained from direct radiation using the monochromatic direct solar flux density equation (Nakajima et al., 1996; Hashimoto et al., 2012), subtracting optical depths caused by ozone and Rayleigh scattering.

To apply a more accurate solar calibration constant ($F_0(\lambda)$) to the

retrieval process, we modified the determination of daily F_0 and its use. In SKYNET, daily F_0 was determined using the improved Langley plot technique (Campanelli et al., 2004; Estelles et al., 2012) from more than 10 points in a day for m_0 (air mass) < 4.5. In addition to the condition for air mass, we used the solar constant (F) only for AOD₅₀₀ ≤ 0.3, because F_0 can be obscured by uncertainty of imaginary refractive index for AOD₅₀₀ > 0.3 due to scattering angle ranging from 3° to 30° for the determination of F_0 , which is smaller than a full range of 3° to 180° (Campanelli et al., 2004, 2007). Then the outliers were removed from the daily F_0 values using the Chauvenet criterion during the measurement period. Instead of using a single F_0 for the entire period, monthly mean calculated from the daily F_0 values was used by month after confirming no significant filter degradation.

The following are our data processing procedures: (1) Cloud-contaminated data were removed using a cloud-screening algorithm for direct and diffuse AODs from SKYNET (CSDD; Choi et al., 2020a). The CSDD consists of spectral- and temporal-stability tests depending on Ångström exponent (AE) at the first stage, and the temporal-smoothness test at the second stage. Some 15.3% of the original data were eliminated as being cloud-contaminated. Although both direct and diffuse AODs were available, we used diffuse AODs only, which are retrieval products, because we should use other retrieval products, such as single scattering albedo (SSA), to estimate major components of aerosols. (2) We generally adopted AERONET level 2 inversion criteria (Holben et al., 2006; Sinyuk et al., 2020) including the solar zenith angle ≥ 50°, to ensure the quality of retrieval products. For the threshold of retrieval errors, we used the fixed value of 0.07 suggested by Khatri et al. (2014), instead of a dynamic value of AERONET that varies from 0.05 to 0.08, depending on AOD. (3) The AERONET level 2 inversion employs the criterion of AOD ≥ 0.4 for SSA (Holben et al., 2006; Sinyuk et al., 2020). However, this criterion is too strict at the study site, because AOD is generally lower than 0.4. Thus, we lowered the AOD threshold for SSA to 0.2, because when AOD ≥ 0.2, the mean error between the retrieval and measurement values of the SSA is about 1%, while when AOD decreases below 0.2, it becomes significantly larger (Dubovik et al., 2000; Hashimoto et al., 2012; Choi and Ghim, 2016). (4) Hourly data were calculated from all-point measurements for each hour, whereas daily means were calculated from hourly data when three or more data points were available. Monthly means and medians were obtained from daily means, but median values were considered valid only when more than four daily means were available. The total number of daily means for retrieval products except SSA was 937, while the total for SSA was 792, because of the additional criterion described in the procedure (3).

2.2. Study site and period

Skyradiometer measurement was conducted on the rooftop of a five-story building on a hill about 35 km southeast of the center of Seoul (Fig. 1). The site is located in a horseshoe-shaped forested valley with westward-facing slopes; to the west side is a rural area with small-sized buildings, farmland, and open spaces scattered on the sides of a four-lane road and a river. Because there are no major sources nearby, except for a four-lane road running about 1.4 km to the west, the site is ideal to monitor the transport of air pollutants from Seoul and/or the Asian Continent associated with prevailing westerlies, as well as the secondary formation due to photochemical reactions (Choi and Ghim, 2016; Lee et al., 2016). Information on meteorological parameters were obtained from the Seoul Metropolitan Office of Meteorology (37.27° N, 126.99° E, 34.1 m asl; Fig. 1), about 26 km west-southwest of the study site.

The study period was 10 years from March 2007 to February 2017. The measurement was conducted except for four periods including six months between July 2011 and January 2012 for inspection and maintenance. During the study period, PM₁₀ concentration in the Seoul Metropolitan Area, which includes Seoul proper and its neighboring satellite cities (such as Yongin; Fig. S1 in the Supplement), tended to

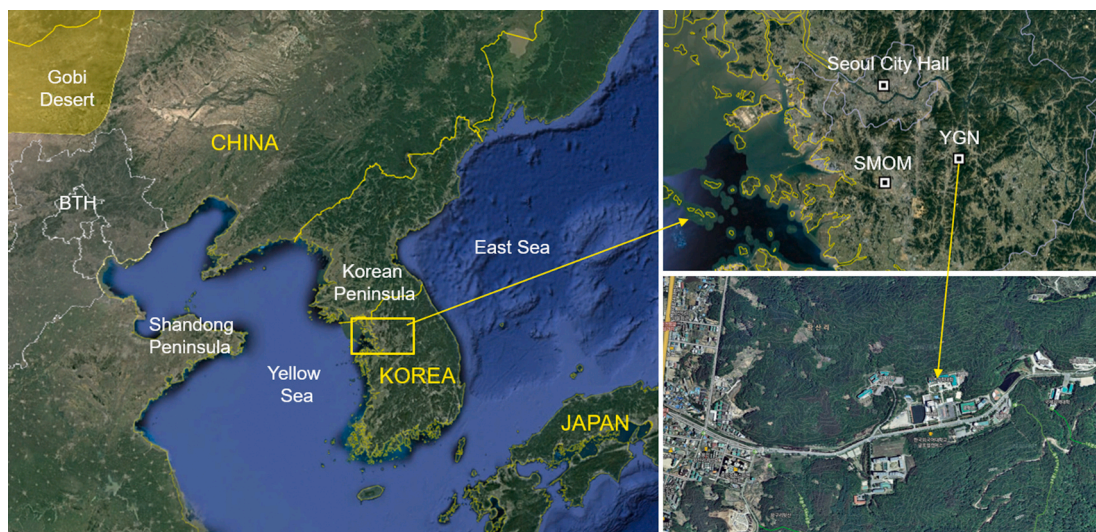


Fig. 1. Location of the Yongin (YGN) study site at the Global Campus of Hankuk University of Foreign Studies. The Seoul Metropolitan Office of Meteorology (SMOM) is about 26 km west-southwest of the study site. The left panel shows potential source regions in China, including the Beijing-Tianjin-Hebei (BTH) region.

decrease due largely to meteorology, especially for the last few years, but also to emission regulations (Kim et al., 2017; Kim and Lee, 2018; Seo et al., 2018). Decreasing trends in emissions and concentrations of major pollutants that have been widely observed in China in recent years (Li et al., 2017; Wang et al., 2017; Zheng et al., 2018; Zhai et al., 2019) should have contributed to this decrease.

2.3. Total potential source contribution function (TPSCF)

The total potential source contribution function analysis with multiple heights was performed (Cheng et al., 1993; Biegalski and Hopke, 2004; Guo et al., 2015), because the receptor site is a column from surface to the top of the atmosphere. Backward trajectories were calculated using the Hybrid Single Particle Lagrangian Integrated Trajectory (HYSPPLIT) 4 model (Draxler et al., 1999). The meteorological data were from the $1^\circ \times 1^\circ$ Global Data Assimilation System (GDAS) archive at 3 h intervals. Trajectories starting at three different heights of 500 m, 1000 m, and 1500 m above the study site at 09:00 LST (0000 UTC) were traced back every hour for 5 days. The trajectory segment endpoints were assigned to the cells of $0.5^\circ \times 0.5^\circ$ geographic coordinates with latitude (i) and longitude (j), and the number of the endpoints within the grid cell was counted. It was noted that the uncertainty of single backward trajectory was similar to, or larger than, 20% of the travel distance (Stohl, 1998; Gebhart et al., 2005). However, the uncertainties in accumulated backward-trajectory endpoints become much smaller, because random errors in the single calculations can be diminished with increasing the number of calculations (Gebhart et al., 2005; Jeong et al., 2017).

The TPSCF at the ij th grid cell can be calculated by the following:

$$\text{TPSCF}_{ij} = \frac{\sum_k m_{ij}^k}{\sum_k n_{ij}^k}$$

where n_{ij}^k is the total number of the endpoints over the ij th grid cell for height k , and m_{ij}^k is the number of endpoints corresponding to certain values of the aerosol optical properties over the same grid cell for the same height. If the total number of trajectory segment endpoints in a particular cell ($\sum_k n_{ij}^k$) is small, the TPSCF value may be biased, especially when these trajectory segments result in the specified ranges of the optical properties at the receptor site. To reduce the effect of abnormal and large values of TPSCF $_{ij}$ with low $\sum_k n_{ij}^k$, a weight function for $\sum_k n_{ij}^k$ suggested by Guo et al. (2015) was applied as follows:

$$W(\sum_k n_{ij}^k) = \begin{cases} 1, & \text{for } T^{0.7} < \sum_k n_{ij}^k \\ 0.7, & \text{for } T^{0.56} < \sum_k n_{ij}^k < T^{0.7} \\ 0.42, & \text{for } T^{0.42} < \sum_k n_{ij}^k < T^{0.56} \\ 0.17, & \text{for } \sum_k n_{ij}^k < T^{0.42} \end{cases}$$

where T is the total number of trajectories at one endpoint height. We used this weight function primarily because this function was suggested for the TPSCF analysis. However, the use of other weight functions for the PSCF analysis, such as those in Hwang and Hopke (2007), Choi et al. (2010), and Jeong et al. (2017), also gave similar results since we examined the spatial variations in the TPSCF values qualitatively during the TPSCF analysis.

3. Results and discussion

3.1. Monthly variations

Fig. 2 shows the monthly mean variations of aerosol optical properties and meteorological parameters during the study period. SSA is the ratio of scattering efficiency to total extinction efficiency. SSA is high for most aerosols, because they effectively scatter light, but is particularly high for fine-mode aerosols without carbonaceous materials, such as secondary inorganic ions (SII) comprising ammonium sulfate and nitrate. Fine mode volume fraction (FMVF) is the ratio of fine mode to total volume concentration. We used FMVF for the aerosol size parameter instead of the traditionally used AE, because AE does not provide clear information in the intermediate range (1–2), which occurs frequently for atmospheric aerosols (Schuster et al., 2006; Prats et al., 2011). dAAOD is the difference between AAOD $_{400}$ and AAOD $_{870}$, where AAOD is the absorption AOD calculated from AOD multiplied by (1-SSA), and the subscript denotes the wavelength. We used dAAOD along with FMVF to distinguish light-absorbing aerosol types. For example, both mineral dust (MD) and organic carbon (OC) show high dAAOD, but MD mostly exists as coarse-mode aerosols, whereas OC exists as fine-mode aerosols. In fact, absorption AE is generally used for this purpose (Russell et al., 2010, 2014; Giles et al., 2012; Choi et al., 2016). However, we used dAAOD, considering that the uncertainties of SSA from SKYNET tend to be larger at longer wavelengths (Che et al., 2008; Khatri et al., 2016; Mok et al., 2018). Some studies dealing with SKYNET data used AAE only when the correlation between AAOD and

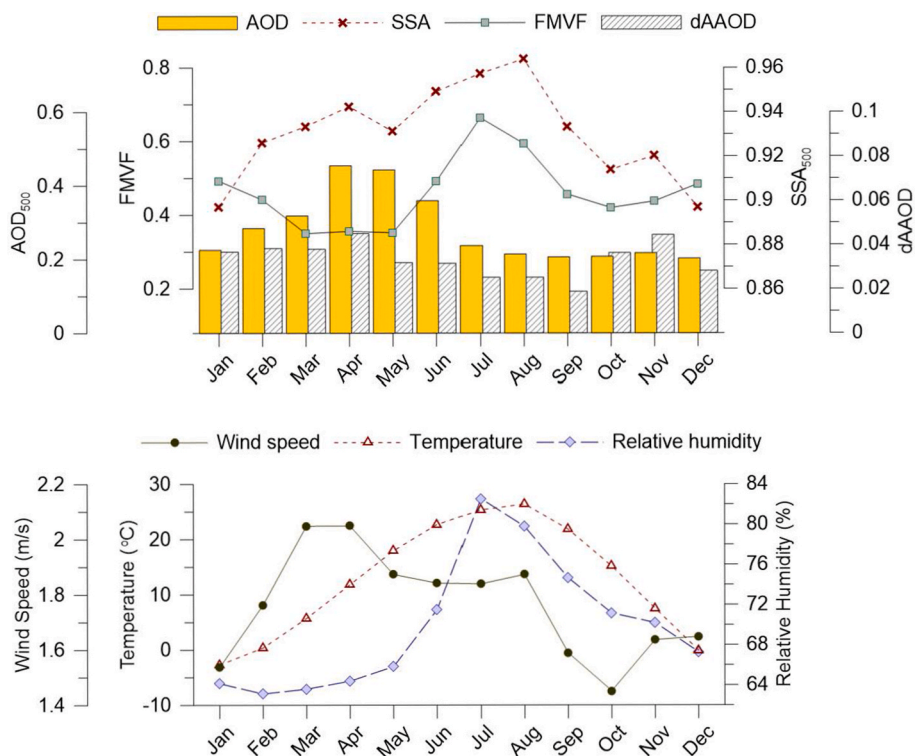


Fig. 2. Monthly mean variations in aerosol optical properties and meteorological parameters.

wavelength was high (Khatri et al., 2010; Irie et al., 2019), but in this case, the number of available data should have been greatly reduced.

Fig. 3 shows how we distinguish aerosol components from optical properties. In Fig. 2, AOD is highest in April along with high SSA and dAAOD, and low FMVF. Highest AOD along with high SSA represents that aerosol loading being highest in the column is mainly due to inorganic ions. High dAAOD accompanying low FMVF suggests the prevalence of MD, which is confirmed by high wind speed and low relative humidity (RH), which are favorable for the generation of mineral and/or fugitive dust (Eck et al., 2005; Kim et al., 2007; Choi et al., 2014; Ghim et al., 2015). Despite some decreases in dAAOD and wind speed, FMVF is still low in May, indicating that the effects of MD remain. However, in the summer months of June to August, in which temperature and RH are high, SSA and FMVF are among the highest. This is attributable to the production of SII, such as ammonium sulfate and nitrate, from active photochemical reactions associated with high temperatures (Pathak et al., 2009; Kim et al., 2015; Lee et al., 2016), and also to their hygroscopic growth under high RH conditions (Choi and Ghim, 2016; Choi et al., 2016). AOD decreases from June to September, as scavenging by

frequent precipitation inhibits the buildup of pollutants, and westerly winds that carry pollutants from the Asian continent are least common (Ghim et al., 2001, 2015). After that, AOD increases until the winter months, but the increase is insignificant. On the other hand, SSA continues to decline, reaching a minimum in December and January, because carbonaceous materials, such as BC and OC, increase with fuel combustion for heating. Unlike SSA, whose variation is relatively simple, FMVF is low in October and increases, while dAAOD is high in November and decreases. Although both BC and OC are present in fine-mode aerosols, BC is mainly emitted from high-temperature combustion, resulting in a higher fraction in smaller size and a lower dAAOD, compared to OC (Russell et al., 2014; Ding et al., 2017). As a result, the variations in FMVF and dAAOD in October and November may be ascribed to OC emitted from biomass burning, including the incineration of crop residues, which is widespread in fall in Northeast Asia (Lim et al., 2012; Shon, 2015; Chen et al., 2017; Yin et al., 2019).

Recently, the application of reanalysis data has become more extensive with the help of improved reanalysis techniques. The monthly variations of major aerosol components derived from the Modern-Era

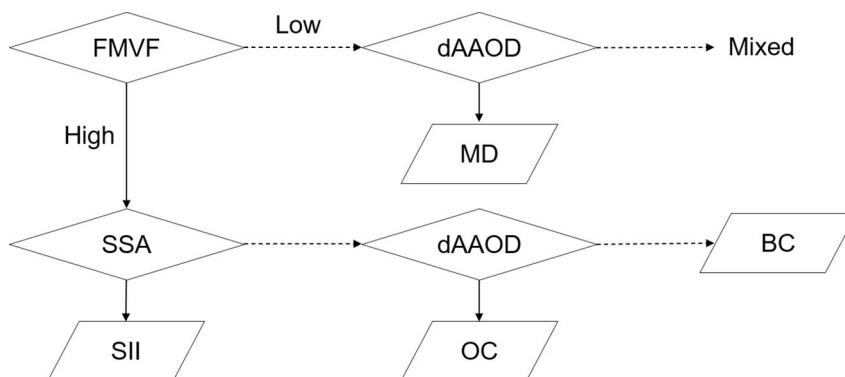


Fig. 3. Flowchart to distinguish major aerosol components from optical properties. For “Mixed,” refer to Choi et al. (2016) and Schuster et al. (2016) for details.

Retrospective analysis for Research and Applications version 2 (MERRA-2; Randles et al., 2017; Buchard et al., 2017) are shown in Fig. S2 in the Supplement. Above all, the variation in total mass concentration agrees well with that in AOD in Fig. 2, and the variations in major components are generally comparable to those mentioned above.

3.2. Long-term trends

Fig. 4 shows the trends in selected aerosol optical properties during the study period. Linear trends were estimated from the Theil-Sen slope (Theil, 1950; Sen, 1968), which has been used to analyze long-term temporal variations in air quality data, because it is robust to outliers, and applicable to non-normal and heteroscedastic data series (Collaud Coen et al., 2013; Munir et al., 2013; Li et al., 2014; Font and Fuller, 2016; Masiol et al., 2017; Coskuner et al., 2018). The Theil-Sen slope was calculated from monthly medians excluding the effects of monthly variations using the R function ‘TheilSen’ included in the package ‘openair’ (Carslaw, 2014).

During the past decade, AOD, SSA, and dAAOD decreased, but FMVF increased. Negative slopes are statistically significant with p -values less than 0.01, whereas the p -value of positive slope for FMVF is larger at 0.09. Although AOD decreases in many parts of the world, variations in other optical properties differ. For example, AOD decreased uniformly for both North America and Europe, but AE trends were opposite (Li et al., 2014). They presumed that both AOD and AE (or FMVF in this study) decreased in Europe, likely because fine-mode anthropogenic emissions reduced, while AOD decreased but AE increased in North America, likely because natural sources, such as those for producing coarse-mode MD, reduced. The increasing trend in FMVF in Fig. 4 indicates that the optical properties in this study are closer to those for North America. The decreasing trend in dAAOD could support the hypothesis that MD reduced because dAAOD increases with MD according to high wavelength dependency of MD on light absorption (Russell et al., 2010, 2014; Giles et al., 2012). This hypothesis is also supported by many studies on Asian dust that have reported the decrease in occurrences over the source region (Ginoux et al., 2004; Wang et al., 2008; Xi and Sokolik, 2015).

Table 1 shows the Theil-Sen slopes of aerosol optical properties by season along with those of meteorological parameters. Whereas monthly medians were used to calculate the slope for optical properties, monthly

Table 1

Theil-Sen slopes of aerosol optical properties and meteorological parameters by season.^{a,b}

	Spring	Summer	Fall	Winter	Overall
(a) Selected optical properties and meteorological parameters					
AOD ₅₀₀	-0.016**	-0.023**	-0.001*	-0.009**	-0.010**
FMVF	0.0023**	0.0069**	-0.0046**	0.0037**	0.0028 ⁺
SSA ₅₀₀	-0.0017**	-0.0035 ⁺	-0.0013	-0.0032**	-0.0021**
dAAOD	-0.0016**	-0.0032**	-0.0026**	-0.0009**	-0.0015**
WS	0.002	0.019**	0.020**	0.049**	0.018**
Temp	0.17*	0.13**	0.09*	0.07	0.11**
RH	-0.84**	-0.29**	-0.77**	-1.23**	-0.48**
Precip ^c	-3.3**	-21.4**	-3.0*	1.6**	-1.0
(b) Scattering and absorption AODs					
SAOD ₅₀₀ ^d	-0.013**	-0.014**	0.005**	-0.002	-0.008**
AAOD ₅₀₀	-0.0004	-0.0003	0.0006	0.0000**	0.0001

^a p -value: ** $p < 0.01$, * $p < 0.05$, + $p < 0.1$.

^b WS, wind speed in m/s/year; Temp, temperature in °C/year; RH, relative humidity in %/year; Precip, precipitation in mm/year.

^c Based on monthly total, while the slopes for other meteorological parameters were calculated based on monthly means.

^d Scattering AOD calculated from AOD multiplied by SSA at 500 nm.

means were used for meteorological parameters except precipitation (for which monthly totals were used), because there was no missing data. If MD has reduced, the variations in indicators, such as decrease in dAAOD and increase in FMVF, should be large in spring, but is largest in summer. The decline of AOD is also largest in summer, along with the reduction of the scattering AOD (SAOD). It is probable that the diminution of SII is primarily responsible, but their decrease in hygroscopic growth with temperature rise and RH decrease could also contribute to this reduction of AOD. However, Table 1 exhibits the increase in FMVF, whereas FMVF should be lowered with reducing SII. The lowering of FMVF with reducing SII is likely outweighed by the elevation of FMVF with reducing coarse-mode MD.

The variations of optical properties in spring are similar to those in summer. SII and MD may also diminish in spring although the smaller magnitudes of the slopes indicate that the diminutions are smaller compared to summer. In fall, AOD declines only slightly, while SAOD increases along with lowering of FMVF and dAAOD. SAOD could increase with increasing SII, but in this case, FMVF should be elevated. This elevation of FMVF could be outweighed by the lowering of FMVF

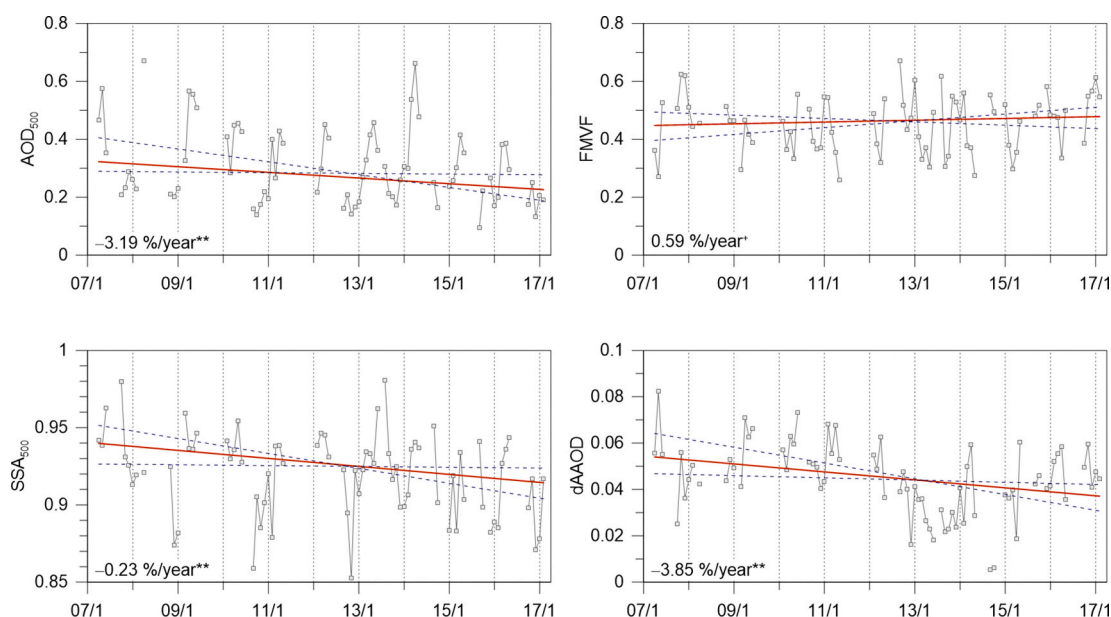


Fig. 4. Temporal variations in monthly medians of aerosol optical properties during March 2007 to February 2017. Red solid and dotted lines denote the Theil-Sen slope and 95 % confidence intervals, respectively. The percent changes are shown in the lower left corner along with the p -value: ** $p < 0.01$, * $p < 0.05$, + $p < 0.1$.

with reduction of OC, which was noted as a key species for the variations in FMVF and dAAOD in October and November in Section 3.1. The reduction of OC is also plausible, in that it lowers dAAOD as well. However, such reduction should diminish AAOD, which contradicts the positive trend of AAOD in Table 1, although that trend is statistically insignificant. The variations of optical properties in winter are similar to those in spring and summer, except that AAOD is not decreased. The reduction of SII still seems effective in diminishing AOD. However, the elevation of FMVF cannot be explained by the reduction of MD, because AAOD is not decreased. Section 3.1 noted that the roles of carbonaceous materials, such as BC and OC, are important in the variations of optical properties during the winter season. Most variations of optical properties in winter, including the elevation of FMVF and the declines of SSA and dAAOD, can result from the increase of BC. The optical properties of OC are similar to those of BC, but dAAOD increases with increasing OC, which is different from Table 1.

Table 2 lists selected trends in major aerosol components identified from those in optical properties. AOD declined in all seasons, and the reduction of SII was significant, except in fall. Except for fall, FMVF was elevated, which was interpreted as a reduction in MD in spring and summer, and an increase in BC as well in winter, resulting in the decline of dAAOD. In the fall, the slope of SAOD was positive in contrast to other seasons, which was presumed to be due to an increase in SII; and the diminutions of FMVF and dAAOD were presumed to be caused by the reduction of OC. As mentioned earlier, the decline of AOD during the study period could be easily understood from the variations in pollutant concentrations in both China and Korea (e.g., Seo et al., 2018; Zhai et al., 2019). On the other hand, the variations in aerosol components are uncertain in Korea, because of a few measurement data without a distinct trend (Kim and Lee, 2018). Therefore, the Theil-Sen slopes of major aerosol components calculated from MERRA-2 and the Tropospheric Chemical Reanalysis version 2 (TCR-2; Miyazaki et al., 2020) for the study period are presented in Table 3. The overall variations in Table 3(a) are in good agreement with those in Table 2, such as decreases in MD and sulfate and insignificant trends in OC and BC. In the case of MD, even the seasonal variations are the same. SII increase in fall of Table 2 is different from that of Table 3(a), but the magnitude of the negative slope is the smallest in Table 3(b). However, the detailed seasonal variations in OC and BC in Table 3(a) are different from those in Table 2.

3.3. Potential source regions

Fig. 5 shows the TPSCF analysis results for the upper and lower 25th percentile of aerosol optical properties. The threshold values of the upper and lower 25th percentiles were 0.44 and 0.18 for AOD, 0.95 and 0.89 for SSA, 0.55 and 0.34 for FMVF, and 0.06 and 0.03 for dAAOD, respectively. In Sections 3.1 and 3.2, AOD can be high due to both anthropogenic and natural emissions, producing major components of aerosols such as SII, carbonaceous materials, and MD. Potential source regions for the upper 25th percentile of AOD are distributed mostly over the Yellow Sea, between the east coast of China centered on the Shandong Peninsula and the west coast of the central Korean Peninsula

Table 2

Selected trends in major aerosol components estimated from those in aerosol optical properties by season.^{a,b}

	Spring	Summer	Fall	Winter	Overall
MD	↓	↓		↓	↓
SII	↓	↓	↑	↓	↓
OC			↓		
BC				↑	

^a MD, mineral dust; SII, secondary inorganic ions; OC, organic carbon; BC, black carbon.

^b Vertical arrow direction denotes increase (↑) or decrease (↓).

Table 3

Theil-Sen slopes of major aerosol compositions from MERRA-2 and TCR-2.^a

	Spring	Summer	Fall	Winter	Overall
(a) MERRA-2 ^b					
MD	-0.850**	-0.089**	0.061	-0.294**	-0.164**
Sulfate	-0.105**	-0.186**	-0.113**	-0.183**	-0.124**
OC	-0.010	0.048**	0.018**	-0.040**	0.002
BC	0.001	-0.012*	-0.016**	-0.029**	-0.012
(b) TCR-2 ^c					
SII	-0.349**	-0.407**	-0.315**	-0.666**	-0.411**

^a *p*-value: ***p* < 0.01, **p* < 0.05.

^b Using monthly concentrations at the surface with horizontal resolution of 0.05° × 0.625° (<https://daac.gsfc.nasa.gov>).

^c Using monthly concentrations calculated from 2-h concentrations at the surface with horizontal resolution of 1.1° × 1.1° (<https://ebcrpa.jamstec.go.jp/trcr2/download.html#1-2>).

(Fig. 5a). The Beijing-Tianjin-Hebei (BTH) region to the northwest of the Shandong Peninsula is a representative polluted area in China (Zhang et al., 2015; Zheng et al., 2016; Guo et al., 2017). The distribution of potential source regions over the Yellow Sea, which is downwind of the highly polluted BTH region, indicates that secondary formation during the long-range transport from the northwest played an important role in elevating AOD. In the case of the lower 25th percentile of AOD, the TPSCF values are high to the north-northwest and northeast of the study site, which are representative low-pollution areas around the Korean Peninsula (Zhang et al., 2009; Ghim et al., 2001).

While AOD exhibits the total amount of aerosol loading in the column, FMVF, SSA and dAAOD signify certain properties of aerosols. FMVF increases when SII, BC, or OC are high, but declines when MD or sea salt is high. In the case of low FMVF, the TPSCF values are high in the west coast off the central Korean Peninsula, and broadly higher to the northwest including the Gobi Desert (Fig. 5d), probably associated with the effects of sea salt and MD (represented by Asian dust), respectively. TPSCF values to the northwest are not noticeable compared to the west coast off the central Korean Peninsula, likely because Asian dust is often mixed with various species of fine-mode aerosols (Mori et al., 2003; Arimoto et al., 2004; Bates et al., 2004; Sullivan et al., 2007), which lowers TPSCF values by increasing FMVF. On the other hand, sea salt concentration is generally high when AOD is low (Smirnov et al., 2002, 2011). Because high-concentration sea salt is rarely mixed with fine-mode species, the TPSCF values could be high for the case of low FMVF by emphasizing the effects of sea salt. dAAOD increases with MD or OC, and decreases with BC. In Fig. 5g for high dAAOD, the TPSCF values are high along the route both from the northwest where MD is transported and from the Shandong Peninsula. The latter is possibly due to the contribution of primary and secondary OC resulting from the incineration of crop residues over the farmland on the east coast of China (Chen et al., 2017; Yin et al., 2019).

The TPSCF values are high in the eastern Korean Peninsula and over the East Sea in Fig. 5c, e, and h for high FMVF and SSA and low dAAOD, respectively, which are the characteristics of optical properties in summer (Fig. 2). Compared to Fig. 5a and g, the effects of local emissions stand out because of the typical summer wind patterns with decreasing westerly winds that carry pollutants from the Asian Continent. In Section 3.1, it was mentioned that high FMVF and SSA is caused by active production of SII, but high FMVF and low dAAOD is associated with high concentration of BC. Whereas BC emissions from fuel combustion increase in winter for heating, those from vehicles have small seasonal variations, and the proportion of BC could be elevated when AOD declines in summer. Since a large portion of BC is locally emitted (Ghim et al., 2017; Zheng et al., 2018), the TPSCF values in Fig. 5c and h are high to the east of the study site, instead of the west side where the effects of long-range transport are larger. On the other hand, the TPSCF values in Fig. 5e for high SSA are high both to the east and on the west coast of the central Korean Peninsula, because SII are produced from

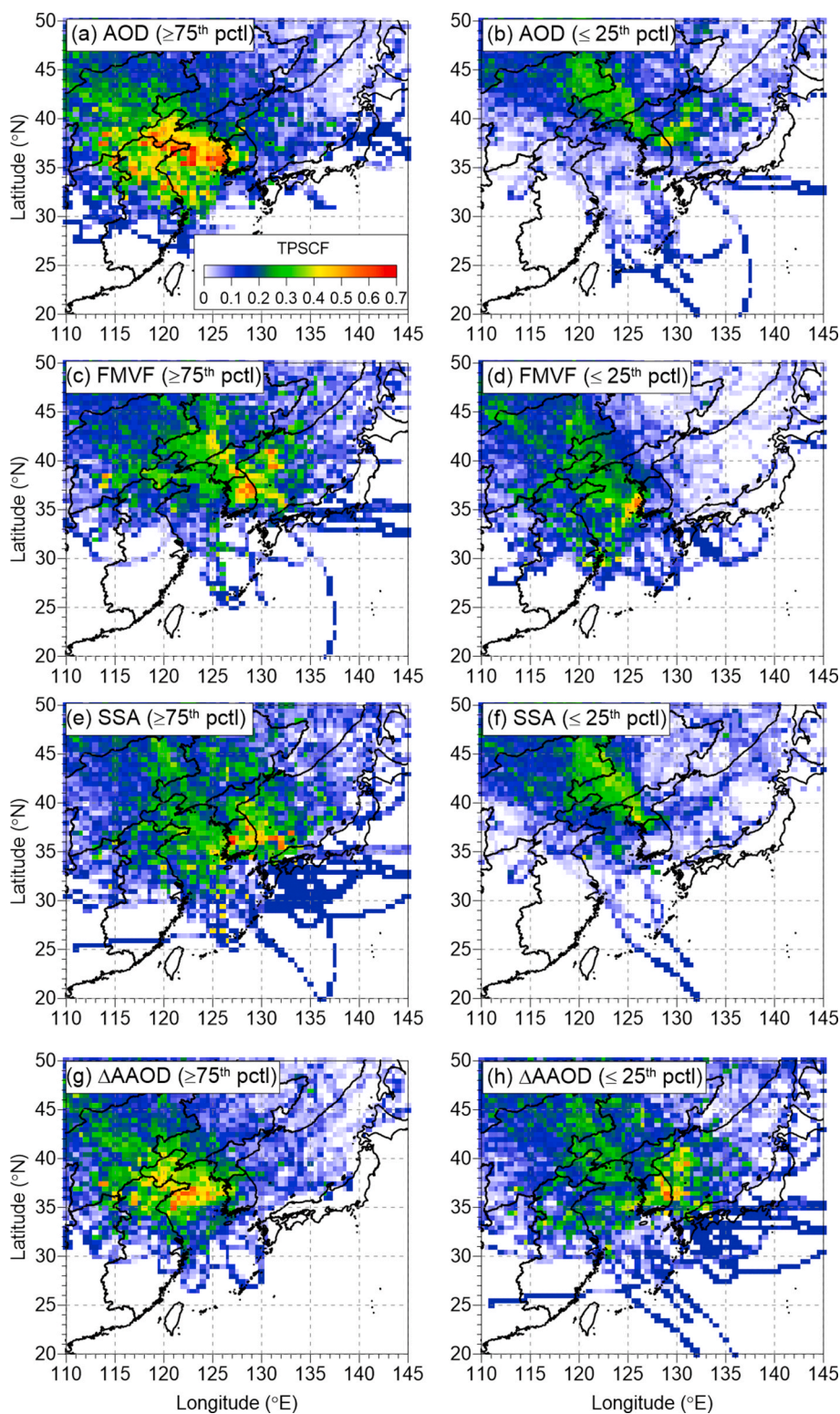


Fig. 5. Potential source regions identified by TPSCF for the upper and lower 25th percentiles (pctls) of aerosol optical properties.

long-range transported pollutants as well as locally emitted ones. In Fig. 5f for low SSA, the TPSCF values are high to the north-northwest as shown in Fig. 5b for low AOD, but not high to the northeast over the East Sea. Considering a low SSA in winter (Fig. 2), this is attributable to the Siberian-high pressure system that generally dominates to the northwest in winter (Lee and Park, 1996; Jhon and Lee, 2004), and to the trajectories from the northeast being rare.

4. Summary and conclusions

The variations in aerosol optical properties from the Yongin SKYNET (YGN) site, downwind of metropolitan Seoul under prevailing westerlies, were analyzed for 10 years from March 2007 to February 2017. Monthly variations and long-term trends of major aerosol components were estimated from optical properties, such as AOD, FMVF, SSA, and Δ AAOD. The validity of the estimation was assessed by comparing the

results with those from previous studies. Potential source regions for high and low values of optical properties were searched to locate the possible origins of relevant pollution phenomena.

Monthly variations in aerosol characteristics estimated from the optical properties were mostly consistent with the previous studies based on *in-situ* measurement data. A representative example was similar variations in AOD and PM. The prevalence of MD was manifested as low FMVF and high dAAOD in spring, and the production of SII was manifested as high SSA and FMVF in summer. In winter, BC emissions from fuel combustion for heating lowered SSA and dAAOD, and elevated FMVF. The effect of MD was presumed to persist in May albeit decreases in dAAOD and wind speed, considering low FMVF. Elevation of dAAOD along with relatively low FMVF in October and November was attributed to increase in OC emissions from biomass burning.

While many studies reported the reduction of PM in Northeast Asia, AOD decreased as well in the trend analysis using the Theil-Sen slope. In most seasons, FMVF was elevated and dAAOD was declined due to the reduction of MD, and SSA and SAOD were lowered due to the diminution of SII. Despite decreases in both coarse-mode MD and fine-mode SII, FMVF was generally raised. It may be interpreted that the declines of FMVF and dAAOD in fall were due to OC decrease, and that the elevation of FMVF and the reduction in SSA and dAAOD in winter were due to BC increase. Because *in-situ* measurement data for aerosol components were insufficient in Korea during the study period, the trend analysis results were compared with those from reanalysis data. The overall variations in major aerosol components were in good agreement, but for OC and BC, detailed seasonal trends differed.

The distribution of potential source regions from the TPSCF analysis exhibited that the effects of long-range transport were important in the variation of AOD. Accordingly, the TPSCF values for high AOD were mainly high over the Yellow Sea downwind of BTH, a representative polluted area in China, indicating that secondary formation was a major factor in elevating AOD. On the other hand, the TPSCF values for other optical properties were high when the individual property varied independently; for example, the TSCF values for low FMVF were high to the west-southwest over the Yellow Sea as the effect of sea salt stood out while AOD was low. For the specific case of high FMVF, high SSA, or low dAAOD, the TPSCF values tended to be high in the eastern Korean Peninsula and over the East Sea, as the effects of local emissions became larger over those of long-range transport.

The study period from March 2007 to February 2017 is a decade during which numerous measures to reduce air pollutants were implemented in both Korea and China. Although aerosol components are presumed to vary significantly, *in-situ* measurement data are mostly insufficient to determine the variations in aerosol components. In this study, the variations in major aerosol components were investigated using optical properties. Whereas AOD variations successfully revealed the overall characteristics of PM, in some cases, the variations in optical properties were not clearly related to those in aerosol components. It is uncertain whether such ambiguity was derived from the optical properties themselves, or from the relationship between optical properties and aerosol components. Further studies are warranted to ensure the reliability of aerosol components from optical properties.

CRedit authorship contribution statement

Yongjoo Choi: Conceptualization, Methodology, Investigation, Data curation, Writing - original draft. **Young Sung Ghim:** Conceptualization, Validation, Writing - review & editing, Supervision.

Declaration of competing interest

The authors declare that they have no known competing financial interests or personal relationships that could have appeared to influence the work reported in this paper.

Acknowledgements

This study was supported by National Research Foundation of Korea (NRF) grants funded by the Korea government (MSIT) (NRF-2018R1C1B6008004 and NRF-2019R1F1A1058127), and the Hankuk University of Foreign Studies Research Fund. We thank the Korea Meteorological Administration for providing meteorological data through <http://www.kma.go.kr/weather/observation/currentweather.jsp> (in Korean).

Appendix A. Supplementary data

Supplementary data to this article can be found online at <https://doi.org/10.1016/j.atmosenv.2020.117991>.

References

- Arimoto, R., Zhang, X.Y., Huebert, B.J., Kang, C.H., Savoie, D.L., Prospero, J.M., Sage, S.K., Schloesslin, C.A., Khaing, H.M., Oh, S.N., 2004. Chemical composition of atmospheric aerosols from Zhenbeitai, China, and Gosan, South Korea, during ACE-Asia. *J. Geophys. Res. Atmospheres* 109.
- Arola, A., Eck, T.F., Kokkola, H., Pitkänen, M.R.A., Romakkaniemi, S., 2017. Assessment of cloud-related fine-mode AOD enhancements based on AERONET SDA product. *Atmos. Chem. Phys.* 17, 5991–6001. <https://doi.org/10.5194/acp-17-5991-2017>.
- Bates, T.S., Quinn, P.K., Coffman, D.J., Covert, D.S., Miller, T.L., Johnson, J.E., et al., 2004. Marine boundary layer dust and pollutant transport associated with the passage of a frontal system over eastern Asia. *J. Geophys. Res. Atmospheres* 109 (D19).
- Biegalski, S.R., Hopke, P.K., 2004. Total potential source contribution function analysis of trace elements determined in aerosol samples collected near Lake Huron. *Environ. Sci. Technol.* 38 (16), 4276–4284.
- Buchard, V., Randles, C.A., Da Silva, A.M., Darmenov, A., Colarco, P.R., Govindaraju, R., Ferrare, R., Hair, J., Beyersdorf, A.J., Ziemba, L.D., Yu, H., 2017. The MERRA-2 aerosol reanalysis, 1980 onward. Part II: evaluation and case studies. *J. Clim.* 30, 6851–6872.
- Carlsaw, D.C., 2014. The Openair Manual — Open-Source Tools for Analyzing Air Pollution data. Manual for Version 1.0. King's College London.
- Campanelli, M., Nakajima, T., Olivieri, B., 2004. Determination of the solar calibration constant for a sun-sky radiometer: proposal of an *in-situ* procedure. *Appl. Optic.* 43, 651–659.
- Campanelli, M., Estellés, V., Tomasi, C., Nakajima, T., Malvestuto, V., Martínez-Lozano, J.A., 2007. Application of the SKYRAD Improved Langley plot method for the *in situ* calibration of CIMEL Sun-sky photometers. *Appl. Optic.* 46, 2688–2702.
- Campanelli, M., Estelles, V., Smyth, T., Tomasi, C., Martínez-Lozano, M.P., Claxton, B., Muller, P., Pappalardo, G., Pietruczuk, A., Shanklin, J., Colwell, S., Wrench, C., Lupi, A., Mazzola, M., Lanconelli, C., Vitale, V., Congeduti, F., Dionisi, D., Cardillo, F., Cacciani, M., Casasanta, G., Nakajima, T., 2012. Monitoring of Eyjafjallajökull volcanic aerosol by the new European SkyNet Radiometers (ESR) network. *Atmos. Environ.* 48, 33–45. <https://doi.org/10.1016/j.atmosenv.2011.09.070>.
- Che, H., Shi, G., Uchiyama, A., Yamazaki, A., Chen, H., Goloub, P., Zhang, X., 2008. Intercomparison between aerosol optical properties by a PREDE skyradiometer and CIMEL sunphotometer over Beijing, China. *Atmos. Chem. Phys.* 8, 3199–3214.
- Chen, J., Li, C., Ristovski, Z., Milic, A., Gu, Y., Islam, M.S., Wang, S., Hao, J., Zhang, H., He, C., Guo, H., Fu, H., Miljevic, B., Morawska, L., Thai, P., Lam, Y.F., Pereira, G., Ding, A., Huang, X., Dumka, U.C., 2017. A review of biomass burning: emissions and impacts on air quality, health and climate in China. *Sci. Total Environ.* 579, 1000–1034.
- Cheng, M.D., Hopke, P.K., Barrie, L., Rippe, A., Olson, M., Landsberger, S., 1993. Qualitative determination of source regions of aerosol in Canadian high Arctic. *Environ. Sci. Technol.* 27 (10), 2063–2071.
- Cheng, Y., Zheng, G., Wei, C., Mu, Q., Zheng, B., Wang, Z., Gao, M., Zhang, Q., He, K., Carmichael, G.R., Pöschl, U., Su, H., 2016. Reactive nitrogen chemistry in aerosol water as a source of sulfate during haze events in China. *Science Advances* 2 (12), e1601530.
- Choi, E., Heo, J.-B., Yi, S.-M., 2010. Apportioning and locating nonmethane hydrocarbon sources to a background site in Korea. *Environ. Sci. Technol.* 44, 5849–5854.
- Choi, S.-H., Ghim, Y.S., Chang, Y.-S., Jung, K., 2014. Behavior of particulate matter during high concentration episodes in Seoul. *Environ. Sci. Pollut. Res.* 21, 5972–5982.
- Choi, Y., Ghim, Y.S., 2016. Estimation of columnar concentrations of absorbing and scattering fine mode aerosol components using AERONET data. *J. Geophys. Res. Atmospheres* 121.
- Choi, Y., Ghim, Y.S., Holben, B.N., 2016. Identification of columnar aerosol types under high aerosol optical depth conditions for a single AERONET site in Korea. *J. Geophys. Res. Atmospheres* 121, 1264–1277.
- Choi, Y., Ghim, Y.S., Kim, S.-W., Yeo, H., 2020a. Development of a cloud-screening algorithm for direct and diffuse AODs from the Skyradiometer Network. *Atmos. Res.* 243, 104997.
- Choi, Y., Kanaya, Y., Park, S.-M., Matsuki, A., Sadanaga, Y., Kim, S.-W., Uno, I., Pan, X., Lee, M., Kim, H., Jung, D.H., 2020b. Regional variability in black carbon and carbon

- monoxide ratio from long-term observations over East Asia: assessment of representativeness for black carbon (BC) and carbon monoxide (CO) emission inventories. *Atmos. Chem. Phys.* 20, 83–98. <https://doi.org/10.5194/acp-20-83-2020>.
- Collaud Coen, M., Andrews, E., Asmi, A., Baltensperger, U., Bukowiecki, N., Day, D., Fiebig, M., Fjaeraa, A.M., Flentje, H., Hyvärinen, A., Jefferson, A., Jennings, S.G., Kouvarakis, G., Lihavainen, H., Lund Myhre, C., Malm, W.C., Mihapopoulos, N., Molenaar, J.V., O'Dowd, C., Ogren, J.A., Schichtel, B.A., Sheridan, P., Virkkula, A., Weingartner, E., Weller, R., Laj, P., 2013. Aerosol decadal trends – Part 1: in-situ optical measurements at GAW and IMPROVE stations. *Atmos. Chem. Phys.* 13, 869–894.
- Coskuner, G., Jassim, M.S., Munir, S., 2018. Characterizing temporal variability of PM_{2.5}/PM₁₀ ratio and its relationship with meteorological parameters in Bahrain. *Environ. Forensics* 19 (4), 315–326.
- Ding, X.X., Kong, L., Du, C.T., Zhazakova, A., Fu, H.B., Tang, X.F., Wang, L., Yang, X., Chen, J.M., Cheng, T.T., 2017. Characteristics of size-resolved atmospheric inorganic and carbonaceous aerosols in urban Shanghai. *Atmos. Environ. Times* 167, 625–641.
- Draxler, R.R., Stunder, B., Rolph, G., Stein, A., Taylor, A., 1999. HYSPLIT4 Users's Guide. US Department of Commerce, National Oceanic and Atmospheric Administration, Environmental Research Laboratories, Air Resources Laboratory.
- Dubovik, O., King, M.D., 2000. A flexible inversion algorithm for retrieval of aerosol optical properties from Sun and sky radiance measurements. *J. Geophys. Res.* 105, 20673–20696. <https://doi.org/10.1029/2000jd900282>.
- Eck, T.F., Holben, B.N., Dubovik, O., Smirnov, A., Goloub, P., Chen, H.B., Chatenet, B., Gomes, L., Zhang, X.Y., Tsay, S.C., Ji, Q., Giles, D., Slutsker, I., 2005. Columnar aerosol optical properties at AERONET sites in central eastern Asia and aerosol transport to the tropical mid-Pacific. *J. Geophys. Res.* 110, D06202.
- Estellés, V., Campanelli, M., Utrillas, M.P., Expósito, F., Martínez-Lozano, J.A., 2012. Comparison of AERONET and SKYRAD4.2 inversion products retrieved from a Cimel CE318 sunphotometer. *Atmos. Meas. Tech.* 5, 569–579.
- Font, A., Fuller, G.W., 2016. Did policies to abate atmospheric emissions from traffic have a positive effect in London? *Environ. Pollut.* 218, 463–474.
- Fu, H., Chen, J., 2017. Formation, features and controlling strategies of severe haze-fog pollution in China. *Sci. Total Environ.* 578, 121–138.
- Gebhart, K.A., Schichtel, B.A., Barna, M.G., 2005. Directional biases in back trajectories caused by model and input data. *J. Air Waste Manag.* 55, 1649–1662.
- Ghim, Y.S., Kim, Y.J., Kim, J.Y., 2001. Influences of air trajectories on the variations of carbon monoxide in major cities in Korea for the year of 1999. *J. Korean Society for Atmos. Environ.* 17, 451–461 (in Korean with English abstract).
- Ghim, Y.S., Chang, Y.-S., Jung, K., 2015. Temporal and spatial variations in fine and coarse particles in Seoul, Korea. *Aerosol Air Qual. Res.* 15, 842–852.
- Ghim, Y.S., Kim, J.Y., Chang, Y.-S., 2017. Concentration variations in particulate matter in Seoul associated with Asian dust and smog episodes. *Aerosol and Air Quality Research* 17, 3128–3140.
- Ghim, Y.S., Choi, Y., Park, J., Kim, S., Bae, C.H., Seo, J., Shin, H.J., Lim, Y.J., Lyu, Y.S., Lee, Y.J., 2019. Overall characteristics of nationwide high PM_{2.5} episodes during 2013–2016. *Journal of Korean Society for Atmos. Environ.* 35 (5), 609–624 (in Korean with English abstract).
- Giles, D.M., Holben, B.N., Eck, T.F., Sinyuk, A., Smirnov, A., Slutsker, I., Dickerson, R.R., Thompson, A.M., Schafer, J.S., 2012. An analysis of AERONET aerosol absorption properties and classifications representative of aerosol source regions. *J. Geophys. Res. Atmospheres* 117 (D17).
- Ginoux, P., Prospero, J.M., Torres, O., Chin, M., 2004. Long-term simulation of global dust distribution with the GOCART model: correlation with North Atlantic Oscillation. *Environ. Model. Software* 19 (2), 113–128.
- Guo, H., Cheng, T., Gu, X., Wang, Y., Chen, H., Bao, F., Shi, S., Xu, B., Wang, W., Zuo, X., Zhang, X., Meng, C., 2017. Assessment of PM_{2.5} concentrations and exposure throughout China using ground observations. *Sci. Total Environ.* 601–602, 1024–1030.
- Guo, Q., Hu, M., Guo, S., Wu, Z., Hu, W., Peng, J., Hu, W., Wu, Y., Yuan, B., Zhang, Q., Song, Y., 2015. The identification of source regions of black carbon at a receptor site off the eastern coast of China. *Atmos. Environ.* 100, 78–84.
- Hamill, P., Giordano, M., Ward, C., Giles, D., Holben, B., 2016. An AERONET-based aerosol classification using the Mahalanobis distance. *Atmos. Environ.* 140, 213–233. <https://doi.org/10.1016/j.atmosenv.2016.06.002>.
- Hashimoto, M., Nakajima, T., Dubovik, O., Campanelli, M., Che, H., Khatri, P., Takamura, T., Pandithurai, G., 2012. Development of a new data-processing method for SKYNET sky radiometer observations. *Atmos. Meas. Tech.* 5, 2723–2737.
- Holben, B.N., Eck, T.F., Slutsker, I., Tanré, D., Buis, J.P., Setzer, A., Vermote, E., Reagan, J.A., Kaufman, Y.J., Nakajima, T., Lavenu, F., Jankowiak, I., Smirnov, A., 1998. AERONET—a Federated instrument network and data archive for aerosol characterization. *Rem. Sens. Environ.* 66, 1–16. [https://doi.org/10.1016/S0034-4257\(98\)00031-5](https://doi.org/10.1016/S0034-4257(98)00031-5).
- Holben, B.N., Tanré, D., Smirnov, A., Eck, T.F., Slutsker, I., Abuhassan, N., Newcom, W. W., Schafer, J.S., Chatenet, B., Lavenu, F., Kaufman, Y.J., Castle, J.V., Setzer, A., Markham, B., Clark, D., Frouin, R., Halthore, R., Karneli, A., O'Neill, N.T., Pietras, C., Pinker, R.T., Voss, K., Zibordi, G., 2001. An emerging ground-based aerosol climatology: aerosol optical depth from AERONET. *J. Geophys. Res.* Atmospheres 106 (D11), 12067–12097.
- Holben, B.N., Eck, T.F., Slutsker, I., Smirnov, A., Sinyuk, A., Schafer, J., Giles, D., Dubovik, O., 2006. Aeronet's Version 2.0 Quality Assurance Criteria, vol. 6408, pp. 6408Q–64114Q.
- Huang, R.J., Zhang, Y., Bozzetti, C., Ho, K.-F., Cao, J.-J., Han, Y., Daellenbach, K.R., Slowik, J.G., Platt, S.M., Canonaco, F., Zotter, P., Wolf, R., Pieber, S.M., Bruns, E.A., Crippa, M., Ciarelli, G., Piazzalunga, A., Schwikowski, M., Abbaszade, G., Schnelle-Kreis, J., Zimmermann, R., An, Z., Szidat, S., Baltensperger, U., Haddad, I.E., Prévôt, A.S.H., 2014. High secondary aerosol contribution to particulate pollution during haze events in China. *Nature* 514 (7521), 218–222.
- Hwang, I., Hopke, P.K., 2007. Estimation of source apportionment and potential source locations of PM_{2.5} at a west coastal IMPROVE site. *Atmos. Environ.* 41, 506–518.
- Irie, H., Hoque, H.M.S., Damiani, A., Okamoto, H., Fatmi, A.M., Khatri, P., Takamura, T., Jarupongsakul, T., 2019. Simultaneous observations by sky radiometer and MAX-DOAS for characterization of biomass burning plumes in central Thailand in January–April 2016. *Atmos. Meas. Tech.* 12, 599–606.
- Jhun, J.G., Lee, E.J., 2004. A new East Asian winter monsoon index and associated characteristics of the winter monsoon. *J. Clim.* 17 (4), 711–726.
- Jeong, U., Kim, J., Lee, H., Lee, Y.G., 2017. Assessing the effect of long-range pollutant transportation on air quality in Seoul using the conditional potential source contribution function method. *Atmos. Environ.* 150, 33–44.
- Ji, D., Li, L., Wang, Y., Zhang, J., Cheng, M., Sun, Y., Liu, Z., Wang, L., Tnag, G., Hu, B., Wen, T., Miao, H., 2014. The heaviest particulate air-pollution episodes occurred in northern China in January, 2013: insights gained from observation. *Atmos. Environ.* 92, 546–556. <https://doi.org/10.1016/j.atmosenv.2014.04.048>.
- Khatri, P., Takamura, T., Shimizu, A., Sugimoto, N., 2010. Spectral dependency of aerosol light-absorption over the east China sea region. *SOLA* 6, 1–4.
- Khatri, P., Takamura, T., Shimizu, A., Sugimoto, N., 2014. Observation of low single scattering albedo of aerosols in the downwind of the East Asian desert and urban areas during the inflow of dust aerosols. *J. Geophys. Res.* 119, 787–802. <https://doi.org/10.1002/2013JD019961>.
- Khatri, P., Takamura, T., Nakajima, T., Estellés, V., Irie, H., Kuze, H., Campanelli, M., Sinyuk, A., Lee, S.M., Sohn, B.J., Pandithurai, G., Kim, S.W., Yoon, S.C., Martínez-Lozano, J.A., Hashimoto, M., Devara, P.C.S., Manago, N., 2016. Factors for inconsistent aerosol single scattering albedo between SKYNET and AERONET. *J. Geophys. Res.* 121, 1859–1877.
- Kim, B.M., Seo, J., Kim, J.Y., Lee, J.Y., Kim, Y., 2016. Transported vs. local contributions from secondary and biomass burning sources to PM_{2.5}. *Atmos. Environ.* 144, 24–36. <https://doi.org/10.1016/j.atmosenv.2016.08.072>.
- Kim, C.H., Choi, Y., Ghim, Y.S., 2015. Characterization of volatilization of filter-sampled PM_{2.5} semi-volatile inorganic ions using a backup filter and denuders. *Aerosol Air Qual. Res.* 15 (814), 280.
- Kim, H.C., Kim, S., Kim, B.U., Jin, C.S., Hong, S., Park, R., Son, S.-W., Bae, C., Bae, M., Song, C.-K., Stein, A., 2017. Recent increase of surface particulate matter concentrations in the Seoul Metropolitan Area, Korea. *Sci. Rep.* 7 (1), 4710.
- Kim, S.-W., Yoon, S.-C., Kim, J., Kim, S.-Y., 2007. Seasonal and monthly variations of columnar aerosol optical properties over east Asia determined from multi-year MODIS, LIDAR, and AERONET Sun/sky radiometer measurements. *Atmos. Environ.* 41, 1634–1651.
- Kim, Y.P., Lee, G., 2018. Trend of air quality in Seoul: policy and science. *Aerosol Air Qual. Res.* 18, 2141–2156.
- KME (Korea Ministry of Environment), 2019. Press Release: Opening of an Intensive Air Quality Monitoring Station for the Gyeonggi Province to Strengthen the Capability of Particulate Matter Monitoring. Air Quality Research Division, National Institute of Environmental Research. May 27 (in Korean).
- Koo, Y.-S., Yun, H.-Y., Choi, D.-R., Han, J.-S., Lee, J.-B., Lim, Y.-J., 2018. An analysis of chemical and meteorological characteristics of haze events in the Seoul metropolitan area during January 12–18, 2013. *Atmos. Environ. Times* 178, 87–100. <https://doi.org/10.1016/j.atmosenv.2018.01.037>.
- Lee, T.Y., Park, Y.Y., 1996. Formation of a mesoscale trough over the Korean Peninsula during an excursion of the Siberian high. *Journal of the Meteorological Society of Japan. Ser. II* 74 (3), 299–323.
- Lee, Y.H., Choi, Y., Ghim, Y.S., 2016. Classification of diurnal patterns of particulate inorganic ions downwind of metropolitan Seoul. *Environ. Sci. Pollut. Res.* 23, 8917–8928.
- Li, J., Carlson, B.E., Dubovik, O., Laci, A.A., 2014. Recent trends in aerosol optical properties derived from AERONET measurements. *Atmos. Chem. Phys.* 14, 12271–12289.
- Li, M., Liu, H., Geng, G., Hong, C., Liu, F., Song, Y., Tong, D., Zheng, B., Cui, H., Man, H., Zhang, Q., He, K., 2017. Anthropogenic emission inventories in China: a review. *National Science Review* 4 (6), 834–866.
- Li, Z., Gu, X., Wang, L., Li, D., Xie, Y., Li, K., Dubovik, O., Schuster, G., Goloub, P., Zhang, Y., Li, L., Ma, Y., Xu, H., 2013. Aerosol physical and chemical properties retrieved from ground-based remote sensing measurements during heavy haze days in Beijing winter. *Atmos. Chem. Phys.* 13, 10171–10183.
- Li, Z., Zhang, Y., Xu, H., Li, K., Dubovik, O., Goloub, P., 2019. The Fundamental aerosol models over China region: a cluster Analysis of the ground-based remote sensing measurements of total columnar atmosphere. *Geophys. Res. Lett.* 46, 4924–4932.
- Lim, S., Lee, M., Lee, G., Kim, S., Yoon, S., Kang, K., 2012. Ionic and carbonaceous compositions of PM₁₀, PM_{2.5} and PM_{1.0} at Gosan ABC Superstation and their ratios as source signature. *Atmos. Chem. Phys.* 12 (4), 2007–2024.
- Masiol, M., Squizzato, S., Formenton, G., Harrison, R.M., Agostinelli, C., 2017. Air quality across a European hotspot: spatial gradients, seasonality, diurnal cycles and trends in the Veneto region, NE Italy. *Sci. Total Environ.* 576, 210–224.
- de Meij, A., Pozzer, A., Lelieveld, J., 2012. Trend analysis in aerosol optical depths and pollutant emission estimates between 2000 and 2009. *Atmos. Environ.* 51, 75–85.
- Mok, J., Krotkov, N.A., Torres, O., Jethva, H., Li, Z., Kim, J., Koo, J.H., Go, S., Irie, H., Labow, G., Eck, T.F., Holben, B.N., Herman, J., Loughman, R.P., Spinei, E., Lee, S.S., Khatri, P., Campanelli, M., 2018. Comparisons of spectral aerosol single scattering albedo in Seoul, South Korea. *Atmos. Meas. Tech.* 11, 2295–2311.
- Mori, I., Nishikawa, M., Tanimura, T., Quan, H., 2003. Change in size distribution and chemical composition of kosa (Asian dust) aerosol during long-range transport. *Atmos. Environ.* 37 (30), 4253–4263.

- Munir, S., Habeebullah, T.M., Seroji, A.R., Gabr, S.S., Mohammed, A.M., Morsy, E.A., 2013. Quantifying temporal trends of atmospheric pollutants in Makkah (1997–2012). *Atmos. Environ.* 77, 647–655.
- Miyazaki, K., Bowman, K., Sekiya, T., Eskes, H., Boersma, F., Worden, H., Livesey, N., Payne, V.H., Sudo, K., Kanaya, Y., Takigawa, M., Ogochi, K., 2020. An updated tropospheric chemistry reanalysis and emission estimates, TCR-2, for 2005–2018. *Earth Syst. Sci. Data Discuss.* <https://doi.org/10.5194/essd-2020-30>.
- Nakajima, T., Tonna, G., Rao, R., Boi, P., Kaufman, Y., Holben, B., 1996. Use of sky brightness measurements from ground for remote sensing of particulate polydispersions. *Appl. Optic.* 35, 2672–2686.
- Nakajima, T., Sekiguchi, M., Takemura, T., Uno, I., Higurashi, A., Kim, D., Sohn, B.J., Oh, S.-N., Nakajima, T.Y., Ohta, S., Okada, I., Takamura, T., Kawamoto, K., 2003. Significance of direct and indirect radiative forcings of aerosols in the East China Sea region. *J. Geophys. Res.: Atmosphere* 108. <https://doi.org/10.1029/2002JD003261>.
- Nakajima, T., Yoon, S.-C., Ramanathan, V., Shi, G.-Y., Takemura, T., Higurashi, A., Takamura, T., Aoki, K., Sohn, B.-J., Kim, S.-W., Tsuruta, H., Sugimoto, N., Shimizu, A., Tanimoto, H., Sawa, Y., Lin, N.-H., Lee, C.-T., Goto, D., Schutgens, N., 2007. Overview of the atmospheric Brown cloud east Asian regional experiment 2005 and a study of the aerosol direct radiative forcing in East Asia. *J. Geophys. Res. Atmospheres* 112 (D24), D24S91. <https://doi.org/10.1029/2007JD009009>.
- NIER (National Institute of Environmental Research), 2009. Studies on Improvement of Equipment Operation and Data Utilization for Intensive Air Quality Monitoring Stations. Inha University, Prepared (in Korean).
- Pathak, R.K., Wu, W.S., Wang, T., 2009. Summertime PM_{2.5} ionic species in four major cities of China: nitrate formation in an ammonia-deficient atmosphere. *Atmos. Chem. Phys.* 9, 1711–1722. <https://doi.org/10.5194/acp-9-1711-2009>.
- Prats, N., Cachorro, V.E., Berjón, A., Toledano, C., De Frutos, A.M., 2011. Column-integrated aerosol microphysical properties from AERONET Sun photometer over southwestern Spain. *Atmos. Chem. Phys.* 11, 12535–12547.
- Randles, C., Da Silva, A.M., Buchard, V., Colarco, P.R., Darmenov, A., Govindaraju, R., Smirnov, A., Holben, B., Ferrare, R., Hair, J., Shinzuka, Y., Flynn, C.J., 2017. The MERRA-2 aerosol reanalysis, 1980 onward. Part I: system description and data assimilation evaluation. *J. Clim.* 30, 6823–6850.
- Russell, P.B., Bergstrom, R.W., Shinzuka, Y., Clarke, A.D., DeCarlo, P.F., Jimenez, J.L., Livingston, J.M., Redemann, J., Dubovik, O., Strawa, A., 2010. Absorption Angstrom Exponent in AERONET and related data as an indicator of aerosol composition. *Atmos. Chem. Phys.* 10, 1155–1169. <https://doi.org/10.5194/acp-10-1155-2010>.
- Russell, P.B., Kacenelenbogen, M., Livingston, J.M., Hasekamp, O.P., Burton, S.P., Schuster, G.L., Johnson, M.S., Knobelspiesse, K.D., Redemann, J., Ramachandran, S., Holben, B., 2014. A multiparameter aerosol classification method and its application to retrievals from spaceborne polarimetry. *J. Geophys. Res. Atmospheres* 119 (16), 9838–9863.
- Schuster, G.L., Dubovik, O., Holben, B.N., 2006. Angstrom exponent and bimodal aerosol size distributions. *J. Geophys. Res.* 111, D07207.
- Schuster, G.L., Dubovik, O., Arola, A., 2016. Remote sensing of soot carbon—Part 1: distinguishing different absorbing aerosol species. *Atmos. Chem. Phys.* 16 (3), 1565–1585.
- Sen, P.K., 1968. Estimates of the regression coefficient based on Kendall's tau. *J. Am. Stat. Assoc.* 63, 1379–1389.
- Seo, J., Park, D.S.R., Kim, J.Y., Youn, D., Lim, Y.B., Kim, Y., 2018. Effects of meteorology and emissions on urban air quality: a quantitative statistical approach to long-term records (1999–2016) in Seoul, South Korea. *Atmos. Chem. Phys.* 18 (21), 16121–16137.
- Shon, Z.H., 2015. Long-term variations in PM_{2.5} emission from open biomass burning in Northeast Asia derived from satellite-derived data for 2000–2013. *Atmos. Environ.* 107, 342–350.
- Sinyuk, A., Holben, B.N., Eck, T.F., Giles, D.M., Slutsker, I., Korokin, S., Schafer, J.S., Smirnov, A., Sorokin, M., Lyapustin, A., 2020. The AERONET Version 3 aerosol retrieval algorithm, associated uncertainties and comparisons to Version 2. *Atmos. Meas. Tech. Discuss.* <https://doi.org/10.5194/amt-2019-474>.
- Smirnov, A., Holben, B.N., Kaufman, Y.J., Dubovik, O., Eck, T.F., Slutsker, I., Pietras, C., Halthore, R.N., 2002. Optical properties of atmospheric aerosol in maritime environments. *J. Atmos. Sci.* 59, 501–523.
- Smirnov, A., Holben, B.N., Eck, T.F., Dubovik, O., Slutsker, I. Coauthors, 2011. Maritime aerosol network as a component of AERONET—first results and comparison with global aerosol models and satellite retrievals. *Atmos. Meas. Tech.* 4, 583–597.
- Stohl, A., 1998. Computation, accuracy and applications of trajectories - a review and bibliography. *Atmos. Environ.* 32, 947–966.
- Sullivan, R.C., Guazzotti, S.A., Sodeman, D.A., Prather, K.A., 2007. Direct observations of the atmospheric processing of Asian mineral dust. *Atmos. Chem. Phys.* 7, 1213–1236.
- Theil, H., 1950. A rank-invariant method of linear and polynomial regression analysis. I, II, III. *Nederl. Akad. Wetensch., Proc.* 53, 386–392, 521–525, 1397–1412, MR 0036489.
- Tian, S., Pan, Y., Liu, Z., Wen, T., Wang, Y., 2014. Size-resolved aerosol chemical analysis of extreme haze pollution events during early 2013 in urban Beijing, China. *J. Hazard Mater.* 279, 452–460.
- Wang, J., Wang, S., Jiang, J., Ding, A., Zheng, M., Zhao, B., Wong, D.C., Zhou, W., Zheng, G., Wang, L., Pleim, J.E., Hao, J., 2014a. Impact of aerosol-meteorology interactions on fine particle pollution during China's severe haze episode in January 2013. *Environ. Res. Lett.* 9 (9), 094002 <https://doi.org/10.1088/1748-9326/9/9/094002>.
- Wang, J., Zhao, B., Wang, S., Yang, F., Xing, J., Morawska, L., Ding, A., Kulmala, M., Kerminen, V.-M., Kujansuu, J., Wang, Z., Ding, D., Zhang, X., Wang, H., Tian, M., Petäjä, T., Jiang, J., Hao, J., 2017. Particulate matter pollution over China and the effects of control policies. *Sci. Total Environ.* 584–585, 426–447.
- Wang, L.T., Wei, Z., Yang, J., Zhang, Y., Zhang, F.F., Su, J., Meng, C.C., Zhang, Q., 2014b. The 2013 severe haze over the southern Hebei, China: model evaluation, source apportionment, and policy implications. *Atmos. Chem. Phys.* 14, 3151–3173.
- Wang, X., Huang, J., Ji, M., Higuchi, K., 2008. Variability of East Asia dust events and their long-term trend. *Atmos. Environ.* 42 (13), 3156–3165.
- Xi, X., Sokolik, I.N., 2015. Dust interannual variability and trend in Central Asia from 2000 to 2014 and their climatic linkages. *J. Geophys. Res. Atmospheres* 120 (23), 12–175.
- Xie, Y.S., Li, Z.Q., Zhang, Y.X., Zhang, Y., Li, D.H., Li, K.T., Xu, H., Zhang, Y., Wang, Y.Q., Chen, X.F., Schauer, J.J., Bergin, M., 2017. Estimation of atmospheric aerosol composition from ground-based remote sensing measurements of Sun-sky radiometer. *J. Geophys. Res. Atmospheres* 122, 498–518.
- Yin, L., Du, P., Zhang, M., Liu, M., Xu, T., Song, Y., 2019. Estimation of emissions from biomass burning in China (2003–2017) based on MODIS fire radiative energy data. *Biogeosciences* 16 (7), 1629–1640.
- Yoon, J., Pozzer, A., Chang, D.Y., Lelieveld, J., Kim, J., Kim, M., Lee, Y.G., Koo, J.H., Lee, J., Moon, K.J., 2016. Trend estimates of AERONET-observed and model-simulated AOTs between 1993 and 2013. *Atmos. Environ. Times* 125 (Part A), 33–47. <https://doi.org/10.1016/j.atmosenv.2015.10.058>.
- Zhai, S., Jacob, D.J., Wang, X., Shen, L., Li, K., Zhang, Y., Gui, K., Zhao, T., Liao, H., 2019. Fine particulate matter (PM_{2.5}) trends in China, 2013–2018: separating contributions from anthropogenic emissions and meteorology. *Atmos. Chem. Phys.* 19 (16), 11031–11041.
- Zhang, Y., Li, Z., Sun, Y., Lv, Y., Xie, Y., 2018. Estimation of atmospheric columnar organic matter (OM) mass concentration from remote sensing measurements of aerosol spectral refractive indices. *Atmos. Environ.* 179, 107–117.
- Zhang, Q., Streets, D.G., Carmichael, G.R., He, K.B., Huo, H., Kannari, A., Klimont, Z., Park, I.S., Reddy, S., Fu, J.S., Chen, D., Duan, L., Lei, Y., Wang, L.T., Yao, Z.L., 2009. Asian emissions in 2006 for the NASA INTEX-B mission. *Atmos. Chem. Phys.* 9, 5131–5153.
- Zhang, Y., Yu, H., Eck, T.F., Smirnov, A., Chin, M., Remer, L.A., Bian, H., Tan, Q., Levy, R., Holben, B.N., Piazzolla, S., 2012. Aerosol daytime variations over North and South America derived from multiyear AERONET measurements. *J. Geophys. Res. Atmospheres* 117, D05211. <https://doi.org/10.1029/2011JD017242>.
- Zhang, Y.-L., Cao, F., 2015. Fine particulate matter (PM_{2.5}) in China at a city level. *Sci. Rep.* 5, 14884. <https://doi.org/10.1038/srep14884>.
- Zheng, B., Tong, D., Li, M., Liu, F., Hong, C., Geng, G., Li, H., Li, X., Peng, L., Qi, J., Yan, L., Zhang, Y., Zhao, H., Zheng, Y., He, K., Zhang, Q., 2018. Trends in China's anthropogenic emissions since 2010 as the consequence of clean air actions. *Atmos. Chem. Phys.* 18, 14095–14111.
- Zheng, Y., Zhang, Q., Liu, Y., Geng, G., He, K., 2016. Estimating ground-level PM_{2.5} concentrations over three megalopolises in China using satellite-derived aerosol optical depth measurements. *Atmos. Environ.* 124, 232–242.